Targeting CALR reduces energy metabolism of esophageal cancer cells and inhibits tumor-associated fibroblast infiltration

YU MIAO[1*], XIAOFEI WANG[2*], FANG HE[1*], FEIXIONG ZHANG[1], YING HUANG[1], YAFANG LAI[3], YUANZHEN WANG[1], LINA ZHANG[1], HUA YIN[1], XIANGKUN MENG[1], HAO LIU[1], WEIQIANG LI[4,5] and SHAOQI YANG[1]

[1]Department of Gastroenterology, General Hospital of Ningxia Medical University, Yinchuan, Ningxia Hui 750004, P.R. China; [2]Department of Pathology, North China University of Science and Technology Affiliated Hospital, Tangshan, Hebei 063000, P.R. China; [3]Department of Gastroenterology, Ordos Central Hospital, Ordos, Inner Mongolia 017000, P.R. China; [4]College of Traditional Chinese Medicine, Ningxia Medical University, Yinchuan, Ningxia Hui 750004, P.R. China; [5]Key Laboratory of Ningxia Ethnomedicine Modernization, Ministry of Education, Ningxia Medical University, Yinchuan, Ningxia Hui 750004, P.R. China

Received December 11, 2024; Accepted March 13, 2025

DOI: 10.3892/ijo.2025.5755

Abstract. Calreticulin (CALR) supports the induction of dendritic cell maturation, which makes it a key target for effective esophageal squamous cell carcinoma (ESCC) immunotherapy. The mechanism of CALR in the immunotherapy of ESCC is not fully studied. The aim of the present study was to explore the contributing role of CALR in ESCC progression. The association of CALR expression with calnexin (CANX) and protein disulfide isomerase A3 (PDIA3) expression in ESCC was analyzed. The functions of CALR in ESCC cells were examined by detection of cell migration, endoplasmic reticulum (ER) stress, mitochondrial function, cytoskeletal remodeling, cell proliferation and apoptosis. The effects of CALR on tumor growth and tumor-associated fibroblast infiltration were examined by subcutaneous xenograft assay. The expression of CALR, CANX and PDIA3 in ESCC tissue significantly increased and the expression of PDIA3 was positively associated with CANX. Overexpression of CALR resulted in enhanced cell proliferation, migration, ER stress, mitochondrial function and cytoskeletal remodeling; knockdown of CALR expression had the opposite effect. In the subcutaneous xenograft assay, knockdown CALR significantly inhibited the growth of esophageal cancer tumors, suppressed the invasion of tumor-associated fibroblasts and decreased the expression of α-smooth muscle actin (α-SMA), fibroblast activation protein (FAP), fibroblast specific protein-1 (FSP1), platelet-derived growth factor and transforming growth factor beta (TGF-β) in tumor tissue. These findings suggested that CALR promotes the progression of ESCC by regulating ER stress and mitochondrial function to mediate ATP production, cytoskeletal remodeling, cell proliferation and apoptosis through CANX and PDIA3. Knockdown CALR significantly inhibited tumor-associated fibroblast infiltration and is a potential drug target for ESCC.

Correspondence to: Dr Weiqiang Li, Key Laboratory of Ningxia Ethnomedicine Modernization, Ministry of Education, Ningxia Medical University, 1160 Shengli Street, Xingqing, Yinchuan, Ningxia Hui 750004, P.R. China
E-mail: lwq200309@163.com

Dr Shaoqi Yang, Department of Gastroenterology General Hospital of Ningxia Medical University, 804 Shengli South Street, Xingqing, Yinchuan, Ningxia Hui 750004, P.R. China
E-mail: shaoqiynh@163.com

*Contributed equally

Key words: esophageal squamous cell carcinoma, calreticulin, endoplasmic reticulum stress, mitochondrial dysfunction, tumor-associated fibroblast

Introduction

Esophageal cancer ranks 11th in terms of incidence (511,000 newly diagnosed cases) as well as seventh in mortality overall (445,000 death cases) in 2022 globally (1). At present, surgical resection, radio- and chemotherapies are the primary therapeutic options for ESCC (2). Nevertheless, the outcome remains unsatisfactory because of limited efficacy and severe adverse effects (3,4). Recent clinical trials have demonstrated that immune-checkpoint inhibitors are promising agents for first-line therapy for advanced ESCC (5-7). The first-line treatment with monoclonal antibodies nivolumab or toripalimab combined with chemotherapy and nivolumab combined with ipilimumab remarkably improves overall survival in comparison with chemotherapy alone (5-7). Nevertheless, 54.2% of patients respond to immunotherapy (8). Thus, probing the molecular mechanisms underlying ESCC is key for developing more effective therapeutic strategies.

Production of reactive oxygen species (ROS) within the endoplasmic reticulum (ER) can promote immunogenic cell death in bladder cancer cells (9). Calreticulin (CALR) is a Ca^{2+}-binding ER protein, which facilitates the folding

of proteins that are secreted and inserted into the plasma membrane (10). The accumulation of unfolded proteins induces ER stress, and sustained ER stress can activate apoptosis signals. These functions are associated with chaperone proteins in the ER, including calnexin (CANX) and protein disulfide isomerase A3 (PDIA3) (11,12). ER serves key roles in protein synthesis and folding, which exhibits high sensitivity to cellular redox dynamics (13). The CANX-CALR cycle restores the ER by monitoring the glycosylation status of ER proteins and promoting the correct folding of newly synthesized proteins (14). Dysregulated disulfide bond formation because of ER stress facilitates ER stress and dysfunction (15). The main function of PDIA3 is to mediate the formation of correct disulfide bonds within the molecules of newborn proteins; therefore, the expression of PDIA3 increases after ER stress (14). IP3R is primarily involved in the regulation of calcium homeostasis in the ER. IP3R regulates the transfer of calcium from the ER to mitochondria by forming a 'quasi-synaptic' mechanism with GRP75-VDAC/mitochondrial calcium uniporter (16,17). The present study aimed to determine whether the IP3R1-GRP75-VDAC1 axis is regulated by CALR.

In healthy cells, CALR functions as a chaperone and Ca^{2+} buffer, which assists correct protein folding within the ER (18). It not only maintains cellular protein homeostasis but also supports Ca^{2+}-mediated processes (adhesin and integrin signals), as well as ensuring normal antigen presentation via major histocompatibility complex (MHC) class I molecules. For example, CALR expression on non-small cell lung cancer cellular membranes is associated with dendritic cell infiltration and triggers the migration and maturation of dendritic cells (19). Tumor cells that succumb to immunogenic cell death exhibit CALR on the surface, which facilitates the uptake of dead cells by phagocytes as well as the onset of antitumor immunity (20,21). CALR/Melanoma antigen gene A3 (MAGE-A3)-infected dendritic cells stimulate $CD8^+$ cytotoxic T cells, and leading to increased secretion of interferon-γ, thereby inducing cytotoxic effects on ESCC cells that express MAGE-A3 (22). Despite this, the biological implications of CALR expression and the mechanisms underlying CALR-mediated effects are unclear in ESCC. Therefore, the present study aimed to assess the biological roles and molecular mechanisms CALR in ESCC.

Materials and methods

CALR gene expression levels in Esophageal squamous cell carcinoma and paired normal tissues by the Gene Expression Profiling Interactive Analysis (GEPIA) database. Differential expression analysis of CALR in tumor and normal tissues and the correlation analysis between CALR and CANX/PDIA3 provided by GEPIA were obtained from gepia.cancer-pku.cn/. Paired Student's t test was used for statistical analysis, and the cut-off was $P<0.01$.

Patients and specimens. In total, 79 ESCC along with paired paracancerous tissue samples (>5 cm distal to tumor lesions) were collected from The General Hospital of Ningxia Medical University (Yinchuan, China) from March 2021 to March 2022. There were 44 males and 35 females, with a mean age of 63.72±10.84 years (range, 46-84 years). The inclusion criteria were patients with esophageal cancer confirmed by postoperative pathological diagnosis who had not received radiotherapy or chemotherapy before surgery. Clinical data were acquired from the clinical data registry.

Immunohistochemical staining. Tissue samples were fixed in 4% paraformaldehyde at room temperature for 12 h, then embedded in paraffin. Cut the tissue into 5 μm slices. Tissue slices were deparaffinized and rehydrated using xylene and graded ethanol, then sealed with endogenous peroxidase and antigen retrieval was performed at 92˚C for 10 min. Samples were incubated with 3% hydrogen peroxide solution at 37˚C for 15 min and 10% goat serum (cat. no. ZLI-9056, Beijing Zhongshan Jinqiao Biotechnology Co., Ltd.) was used for endogenous peroxidase/phosphatase activity blocking at 37˚C for 30 min. Incubation with primary antibodies against CALR (1:200; cat. no. 27298-1-AP; Proteintech Group, Inc.), CANX (1:100; cat. no. BF0515, Affinity Biosciences), and PDIA3 (1:200; cat. no. 15967-1-AP; Proteintech Group, Inc.) was conducted overnight at 4˚C, followed by undiluted horseradish peroxidase (HRP) labeled secondary antibody (cat. no. PV-6000; Beijing Zhongshan Jinqiao Biotechnology Co., Ltd.) incubation at room temperature for 20 min. Slices were visualized utilizing DAB and counterstained in hematoxylin at room temperature for 3 min, followed by examination under an inverted fluorescence microscope (Carl Zeiss GmbH, 400x), and quantified with Image Pro Plus 6.0 software (Media Cybernetics). According to the method of Wang *et al* (23), immunohistochemical staining intensity was scored, 0-3 was classified as low expression of CALR, and 4-12 was classified as high expression of CALR.

Subcutaneous xenograft assay. A total of 106-week-old male BALB/c nude mice (17-21 g) were purchased from Charles River Laboratories, Inc. All animal experiments complied with ARRIVE guidelines. Animals were housed as 20-26˚C, humidity of 40-70%, 12/12-h light/darkness, *ad libitum* water and food. The xenograft tumor model was established by subcutaneous injection of $1x10^7$ KYSE-150 cells (Shanghai Zhongqiao Xinzhou Biotechnology Co., Ltd.) into the upper back. After 21 days, the mice were anesthetized with 50 mg/kg pentobarbital sodium and sacrificed by cervical dislocation following anesthesia and the tissues were collected for further experiments.

Animal histopathological analysis. Tumor tissue was collected, fixed with 4% paraformaldehyde at room temperature for 12 h, embedded in paraffin and cut into 5 μm slices for Masson and reticular fiber staining. For Masson staining, after dewaxing, sections were stained with Weiger's iron hematoxylin at room temperature for 5 min, then differentiated using 1% hydrochloric ethanol. Following rinsing with tap water for 30 min, sections were stained with ponceau acid fuchsin solution at room temperature for 5 min, phosphomolybdate solution at room temperature for 3 min and aniline blue at room temperature for 5 min before addition of 1% glacial acetic acid at room temperature for 1 min and sealing with neutral gum. For reticular fiber staining, the dewaxed slices were oxidized with 0.25% potassium permanganate at room temperature

for 3 min, bleached with 1% oxalic acid, stained with 2.5% iron alum and silver diaminohydroxide, reduced with 10% formaldehyde, stained with 0.2% gold chloride, fixed with 5% sodium thiosulfate at room temperature for 5 min, and sealed with neutral gum. Images were captured under an inverted light microscope (Olympus, 400X magnification).

Cell culture. Human ESCC cell lines KYSE150 and KYSE410 (Shanghai Zhongqiao Xinzhou Biotechnology Co., Ltd.) were cultured in DMEM (Gibco, Thermo Fisher SCIENTIFIC) and maintained in a cell incubator (37˚C, 5% CO_2). Cells were passaged every 2-3 days. 1 μM thapsigargin was used for cell culture to induce ER stress, and DMSO was used as the negative control of thapsigargin.

Transfection. Short hairpin (sh)RNA-CALR#1, 2 and 3 were designed and synthesized by Sangon Biotech (Shanghai) Co., Ltd (cat. no. PLVE4646-1) to knockdown the expression of CALR. KYSE150 or KYSE410 cells were seeded into a 6-well plate at 1x10^5 cells/well and incubated at 37˚C with antibiotic-free DMEM [containing 10% FBS (Gibco, Thermo Fisher SCIENTIFIC)] for 24 h. When the cell confluence reached 70%, Lipofectamine 8,000 transfection kit (cat. no. C0533, Beyotime Institute of Biotechnology) was used to transfect 100 pmol sh-CALR#1, 2 and 3 for each well into cells at 37˚C for 12 h. After replacing medium with complete DMEM and incubating at 37˚C for 48 h, the transfection efficiency was detected by western blotting. The sequences of shRNAs were as follows: sh-CALR#1, 5'-CGTCTACTTCAAGGAGCAGTT-3', sh-CALR#2, 5'-GCAGTTCACGGTGAAACATGA-3'; sh-CALR#3, 5'-GCAAGAACGTGCTGATCAACA-3' and sh-negative control (NC), 5'-GTTCTCCGAACTGTCACTA-3'. CALR overexpression (OE) plasmid was purchased from Sangon Biotech (Shanghai) Co., Ltd. and vector pcDNA 3.1 was used as NC. 2.5 μg plasmid were added into each well, and transfected with Lipofectamine 8000 transfection kit (cat. no. C0533, Beyotime Institute of Biotechnology) at 37˚C for 12 h. Then replacing with complete DMEM and incubating at 37˚C for 48 h before subsequent experimentation.

Wound healing assay. Serum starved KYSE150 or KYSE410 cells were seeded into a 6-well culture plate and grown to 90% confluence. Linear scratch wound was created using sterile 200 μl pipette tips in the cell monolayer. Each well was washed with PBS three times to remove detached cells. Under an inverted light microscope (Carl Zeiss GmbH, 40x), the images were captured for calculating the wound area at 0 and 24 h.

Transwell assay. A single cell suspension of KYSE150 or KYSE410 cells was prepared using serum-free DMEM and 200 μl cell suspension was added to the upper chamber (1.5x10^4 cells). A total of 1 ml DMEM containing 10% FBS was added to the lower chamber. After 24 h incubation at 37˚C, the medium in the upper and lower chambers was discarded and the non-migratory cells remaining in the upper chamber were wiped off with a cotton swab. The upper and lower chambers were washed twice with PBS, and the cells were fixed with 4% paraformaldehyde at room temperature for 20 min and stained with 0.1% crystal violet at room temperature for 30 min. A total of three fields of view were randomly selected under an inverted light microscope (Carl Zeiss GmbH, 200x) and the stained cells were counted manually and photographed.

Detection of intracellular Ca^{2+} concentration. KYSE150 or KYSE410 cells were inoculated in 6-well plates (5x10^5 cells/well) and cultured at 37˚C for 48 h. Thereafter, 1 ml each medium and Flou-4 AM staining working solution (cat. no. #F14201, Invitrogen; Thermo Fisher Scientific, Inc.) were separately added to the cells, followed by incubation at 37˚C for 20 min. The supernatant was removed by suction, and the cells were washed twice with Flou-4 AM staining buffer, followed by addition of 2 ml DMEM. The results were observed under a confocal laser scanning microscope (Carl Zeiss GmbH; magnification, x200).

ER-Tracker Red staining. KYSE150 or KYSE410 cells were incubated with ER-Tracker Red staining solution (cat. no. C1041, Beyotime Institute of Biotechnology) for 30 min at 37˚C. Following removal of ER-Tracker Red staining working solution, the cells were washed with PBS three times, and investigated with a confocal laser scanning microscope (Carl Zeiss GmbH; magnification, x400).

Mito-Tracker Red staining. Mitochondrial network structure was assessed with Mito Tracker Red staining (cat. no. C1049B, Beyotime Institute of Biotechnology). Briefly, KYSE150 or KYSE410 cells were incubated with 100 nM Mito Tracker Red reagent in DMEM for 30 min at 37˚C. Images were acquired under a laser scanning confocal microscope (Carl Zeiss GmbH, x400). The mitochondrial perimeter was quantified using Image J 2X software (National Institutes of Health).

Intracellular ROS level measurement. KYSE150 or KYSE410 cells were treated with 10 μM 2,7-dichlorodi-hydrofluorescein diacetate (cat. no. S0033S; Beyotime Institute of Biotechnology) fluorescent probe for 30 min at 37˚C. Intercellular ROS images were captured under a laser scanning confocal microscope (Carl Zeiss GmbH; magnification, x200).

Immunofluorescent staining. KYSE150 or KYSE410 cells were fixed with 4% paraformaldehyde at room temperature for 1 h. Mouse tissues were fixed in 4% paraformaldehyde at room temperature for 12 h, then embedded in paraffin and cut the tissue into 5 μm slices. Mouse tissue sections were dewaxed with xylene and graded ethanol and permeabilized utilizing Triton X-100. Antigen retrieval was performed under 92˚C for 10 min. Incubated the tissues with 10% goat serum (cat. no. ZLI-9056, Beijing Zhongshan Jinqiao Biotechnology Co., Ltd.) for endogenous peroxidase/phosphatase activity blocking at 37˚C for 30 min. Incubation with primary antibodies against CALR (1:200; cat. no. 27298-1-AP; Proteintech Group, Inc.), CANX (1:100; cat. no. BF0515; Affinity Biosciences) and PDIA3 (1:200; cat. no. 15967-1-AP; Proteintech Group, Inc.) was performed at 4˚C overnight, followed by incubation with Alexa Fluor® 488 Conjugate (cat. no. ZF-0512) and Alexa Fluor® 594 Conjugate (both 1:100; cat. no. ZF-0513; both Beijing Zhongshan Jinqiao Biotechnology Co., Ltd.) at 37˚C for 2 h in the dark. DAPI was utilized for nuclear staining at room temperature for 5 min. All sections were scanned utilizing a confocal laser scanning

microscope (Carl Zeiss GmbH; magnification, x400) and analyzed by Image-Pro Plus 6.0 (MEDIA CYBERNETICS).

Western blotting. Protein was extracted from cells using Whole Cell Lysis Assay kit (cat. no. KGB5303; Nanjing KeyGen Biotech Co., Ltd.) according to the manufacturer's instructions. The protein concentration was measured using a BCA kit. A total of 20 μg protein/lane was separated by 10% SDS-PAGE, transferred to PVDF membranes and blocked with 5% non-fat dry milk at room temperature for 1 h. The blocked PVDF membranes were incubated overnight at 4˚C with primary antibodies against CALR (1:1,000; cat. no. 27298-1-AP; Proteintech Group, Inc.), CANX (1:500; cat. no. BF0515; Affinity Biosciences), PDIA3 (cat. no. 15967-1-AP; Proteintech Group, Inc.), vimentin (cat. no. bs-8533R), N-cadherin (cat. no. bs-1172R), glucose regulatory protein 78 (GRP78) (cat. no. bs-1219R; all BIOSS), α-smooth muscle actin (SMA; cat. no. Bs70000; Biogot Technology Co., Ltd.), fibroblast activation protein (FAP; all 1:1,000; cat. no. bs-5758R; BIOSS), ferroptosis suppressor protein 1 (FSP-1) (1:4,000; cat. no. 20886-1-AP), Platelet-derived growth factor receptors (PDGFR) (cat. no. 13449-1-AP; both Proteintech Group, Inc.), TGF-β (both 1:1,000; cat. no. Ab66043, Abcam). GRP75 (1:20,000; cat. no. 14887-1-AP), Voltage dependent anion channel 1 (VDAC1) (cat. no. 55259-1-AP, both Proteintech Group, Inc.) and inositol 1,4,5-Trisphosphate Receptor (IP3R1) (both 1:2,000; cat. no. DF3000, Affinity Biosciences). The horseradish enzyme labeled secondary antibody (1:5,000; cat. nos. ZB-5301 and ZB-2305; Beijing Zhongshan Jinqiao Biotechnology Co., Ltd.) was added at room temperature for 2 h. The proteins were visualized using the ECL Chemiluminescence detection kit (Applygen Technologies Inc.). The protein bands were analyzed with Quantity One software using β-actin (1:2,000; cat. no. AF7018; Affinity Biosciences) as an internal reference. Relative protein expression was measured with ImageJ 2X software (National Institutes of Health).

Co-immunoprecipitation. Immunoprecipitation kit with Protein A + G Magnetic Beads (cat. no. P2179S, Beyotime Institute of Biotechnology) was used for co-immunoprecipitation assay. A total of $5x10^5$ KYSE150 and KYSE410 cells were fully lysed with 100 μl Lysis Buffer (Beyotime, dilute in a ratio of 1:100), centrifuged at 12,000 x g, at 4˚C for 5 min and supernatant was collected. A total of 500 μl VDAC1 (cat. no. 600-401-882) or IP3R1 antibody (both 1:2,000, cat. no. PA1-901; both Thermo Fisher Scientific, Inc.) or normal IgG working solution was added to 20 μl Protein A + G magnetic beads for incubation at room temperature for 2 h. Sample protein and magnetic beads bound with antibodies or normal IgG were added at a volume ratio of 25:1 and incubated at 4˚C overnight. Magnetic beads were separated and the supernatant was retained for western blotting, as aforementioned.

EdU proliferation assay. The EdU working solution from BeyoClick EdU Cell Proliferation kit with Alexa Fluor 594 (cat. no. C0078S, Beyotime Institute of Biotechnology) was added to transfected cells at 37˚C for 2 h. The cells were incubated with 4% paraformaldehyde and PBS containing 0.3% Triton X-100 at room temperature successively for 15 min. Click Reaction Solution was added at room temperature for 30 min away from light before observation under a fluorescence microscope (magnification, x200).

Caspase-3 activity and apoptosis detection. Following removal of the culture medium, Annexin V-mCherry Binding Buffer, Annexin V-mCherry and GreenNuc Caspase-3 Substrate in Caspase-3 Activity and Apoptosis Detection Kit for Live Cell (cat. no. C1077S, Beyotime Institute of Biotechnology) were added to transfected cells in sequence at room temperature in the dark for 30 min before observation under a fluorescence microscope (x200).

Mitochondrial membrane potential detection. Mitochondrial membrane potential test kit (cat. no. M8650, Beijing Solarbio Science & Technology Co., Ltd.) was used for mitochondrial membrane potential detection. A total of $5x10^5$ cells were cultured in a 6-well plate at 37˚C for 24 h, then 1 ml JC-1 staining solution was added to each well at 37˚C for 20 min. Cells were washed with JC-1 staining buffer twice, 2 ml cell culture DMEM was added to each well for observation under a fluorescence microscope (x400).

NAD^+/NADH assay. NAD^+/NADH Assay kit with WST-8 (cat. no. S0175; Beyotime Institute of Biotechnology) was used to assay NAD^+ and NADH levels. Transfected $5x10^5$ cells were cultured in 6-well plates at 37˚C for 48 h. NAD^+/NADH extract was added to lyse the cells and supernatant was obtained after centrifugation at room temperature and 1,000 x g for 5 min for the determination of the total amount of NAD^+ and NADH. The supernatant was heated in a water bath at 60˚C for 30 min to decompose NAD^+ for the determination of NADH content. A total of 20 μl of sample or gradient diluted standard to each well of the 96-well plate, and then add 90 μl of alcohol dehydrogenase working solution to each well. Following incubation at 37˚C for 10 min in the dark, 10 μl color developing solution was added and incubated at 37˚C for 30 min in the dark. Absorbance at 450 nm was measured to calculate the NAD^+ and NADH content.

ActinRed cytoskeleton staining. A total of $5x10^5$ KYSE150 or KYSE410 cells were fixed with 4% paraformaldehyde at room temperature for 10 min, then washed with PBS containing 0.1% Triton X-100 for 5 min. Cells were incubated with PBS containing 1% BSA at room temperature for 20 min and stained with 1:20 ActinRed (cat. no. KGMP0012, Nanjing KeyGen Biotech Co., Ltd.) at room temperature for 20 min. The staining was observed under a fluorescence microscope (x400) after sealing with DAPI at room for 5 min.

Statistical analysis. All statistical analyses were performed with SPSS 23.0 software (IBM Corp.). Unpaired or paired Student's t-test was utilized to compare two groups. χ^2 test was performed to compute the association between CALR expression and clinicopathological factors. One-way ANOVA followed by LSD post hoc test was used to compare >2 groups. All data are presented as the mean ± SD of three independent experimental repeats. $P<0.05$ was considered to indicate a statistically significant difference.

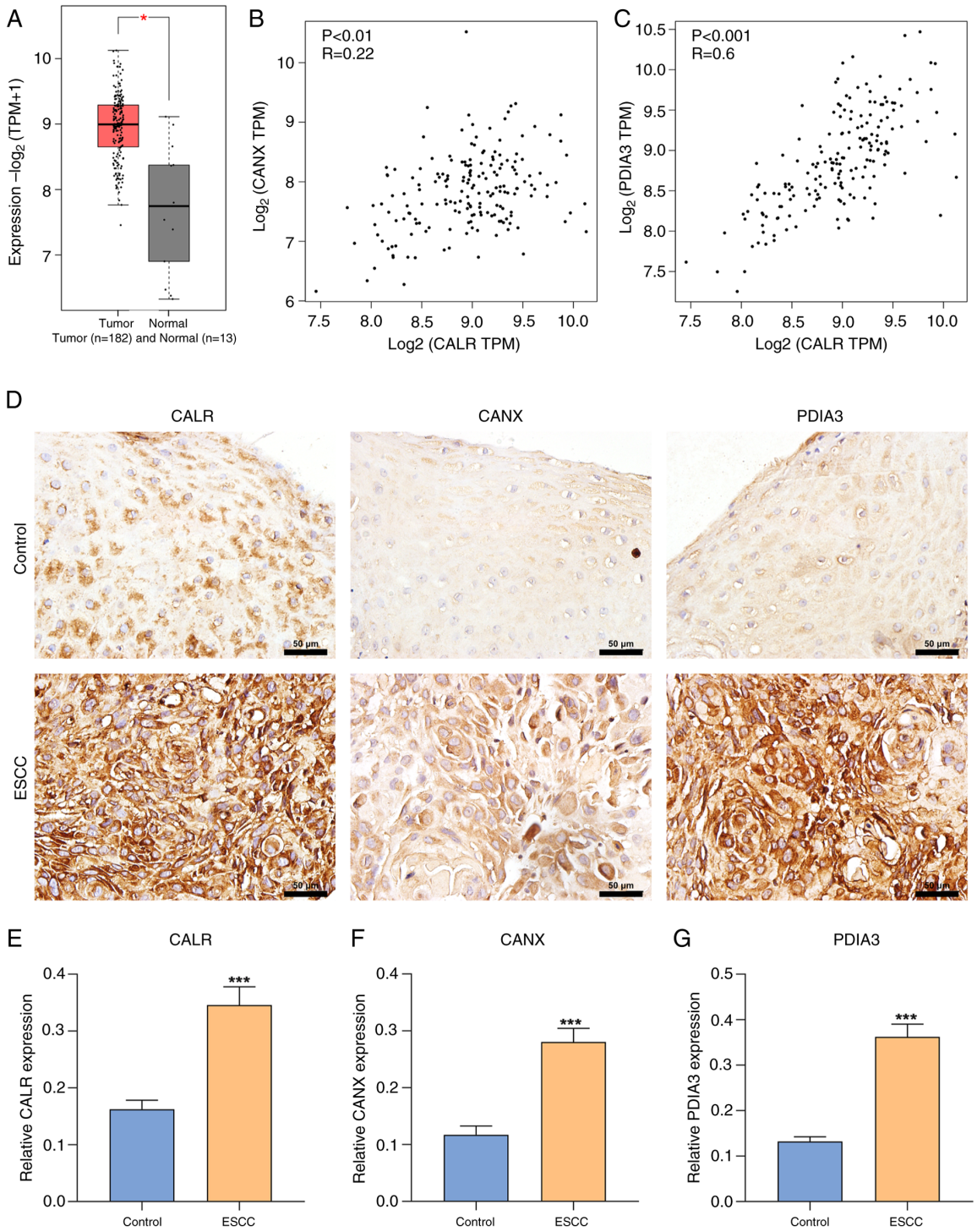

Figure 1. CALR is upregulated in ESCC and positively associated with CANX and PDIA3. (A) RNA expression of CALR in ESCC vs. normal specimens in TCGA-ESCA cohort. Correlation between CALR and (B) CANX and (C) PDIA3 at the RNA level in TCGA-ESCA cohort. (D) Immunohistochemical straining of (E) CALR, (F) CANX and (G) PDIA3 expressions in ESCC and normal tissue. Scale bar, 50 μm. *P<0.05; ***P<0.001 vs. control. CALR, calreticulin; Control, paratumor; ESCC, esophageal squamous cell carcinoma; CANX, calnexin; PDIA3, protein disulfide isomerase A3; ESCA, esophageal carcinoma; TPM, Transcripts Per Million.

Results

CALR is upregulated in ESCC and positively associated with CANX and PDIA3. Using Gene Expression Profiling Interactive Analysis 2 (gepia2.cancer-pku.cn/#index) (24), CALR expression levels were examined in The Cancer Genome Atlas (TCGA)-esophageal carcinoma (ESCA) cohort. Higher CALR expression was observed in ESCA (n=182) in comparison with normal specimens (n=13; Fig. 1A). CALR, CANX and PDIA3 are critical for the proper assembly of MHC class I heavy chains with β2 microglobulin in the lumen of ER 10). In TCGA-ESCA cohort, CALR expression was positively associated with CANX as well as PDIA3 expression (Fig. 1B and C), indicating interactions in ESCC. In total, 79

Table I. Differences in clinicopathological factors in patients with esophageal squamous cell carcinoma with high and low calreticulin expression.

Clinical factor	Total (n=79)	Low (n=18)	High (n=61)	χ^2	P-value
Age, years					
<60	37	8	29	0.054	0.817
≥60	42	10	32		
Sex					
Male	44	11	33	0.277	0.599
Female	35	7	28		
Maximum tumor diameter, cm					
>4	47	14	33	3.234	0.072
≤4	32	4	28		
Tumor location					
Upper thoracic segment	20	4	16	0.123	0.940
Middle thoracic segment	30	7	23		
Lower thoracic segment	29	7	22		
Invasion depth					
Mucous layer	19	5	14	0.332	0.847
Muscle layer	34	8	26		
Mantle layer	26	5	21		
Lymph node metastasis					
Yes	36	4	32	5.123	0.024
No	43	14	29		
TNM stage					
I	13	5	8	8.924	0.023
II	15	6	9		
III	22	5	17		
IV	29	2	27		
Lymphovascular invasion					
Yes	39	5	34	4.347	0.037
No	40	13	27		
Vascular invasion					
Yes	39	4	35	6.872	0.009
No	40	14	26		

ESCC and matched normal tissue samples were included for immunohistochemical straining, which demonstrated significant upregulation of CALR, CANX and PDIA3 in ESCC compared with normal tissue (Fig. 1D-G).

Clinicopathological value of CALR in ESCC. A total of 79 ESCC cases were classified as high (n=61) and low (n=18) expression of CALR and clinicopathological factors were compared. High CALR expression was significantly associated with lymph node metastasis, lymphovascular invasion, TNM stage as well as vascular invasion of ESCC cases (Table I). This indicated the clinicopathological value of CALR during ESCC progression.

CALR is responsible for ESCC migration. sh-CALR#1 sequence exhibited the optimal knockdown effects and was selected for subsequent assays (Fig. 2A-C). Similarly, the transfection efficiency of CALR overexpression plasmid was also verified (Fig. 2D-F). After 24 h, the wound distance was significantly narrower in OE-CALR transfected KYSE150 or KYSE410 cells than controls (Fig. 2G-I). Meanwhile, compared with controls, sh-CALR transfected KYSE150 or KYSE410 cells exhibited significantly wider wound distance. OE-CALR significantly increased migration of KYSE150 or KYSE410 cells in comparison with controls (Fig. 2J-L), whereas migration of sh-CALR transfected KYSE150 or KYSE410 cell cells was significantly decreased, indicating CALR was responsible for migratory ability of ESCC cells.

CALR induces ER stress. Channel functions were evaluated by detecting intracellular Ca^{2+} concentration utilizing Flou-4 Ca^{2+} indicator dye. OE-CALR transfected KYSE150 or KYSE410 cells exhibited enhanced intracellular Ca^{2+} concentration in comparison with controls (Fig. 3A-C). Additionally,

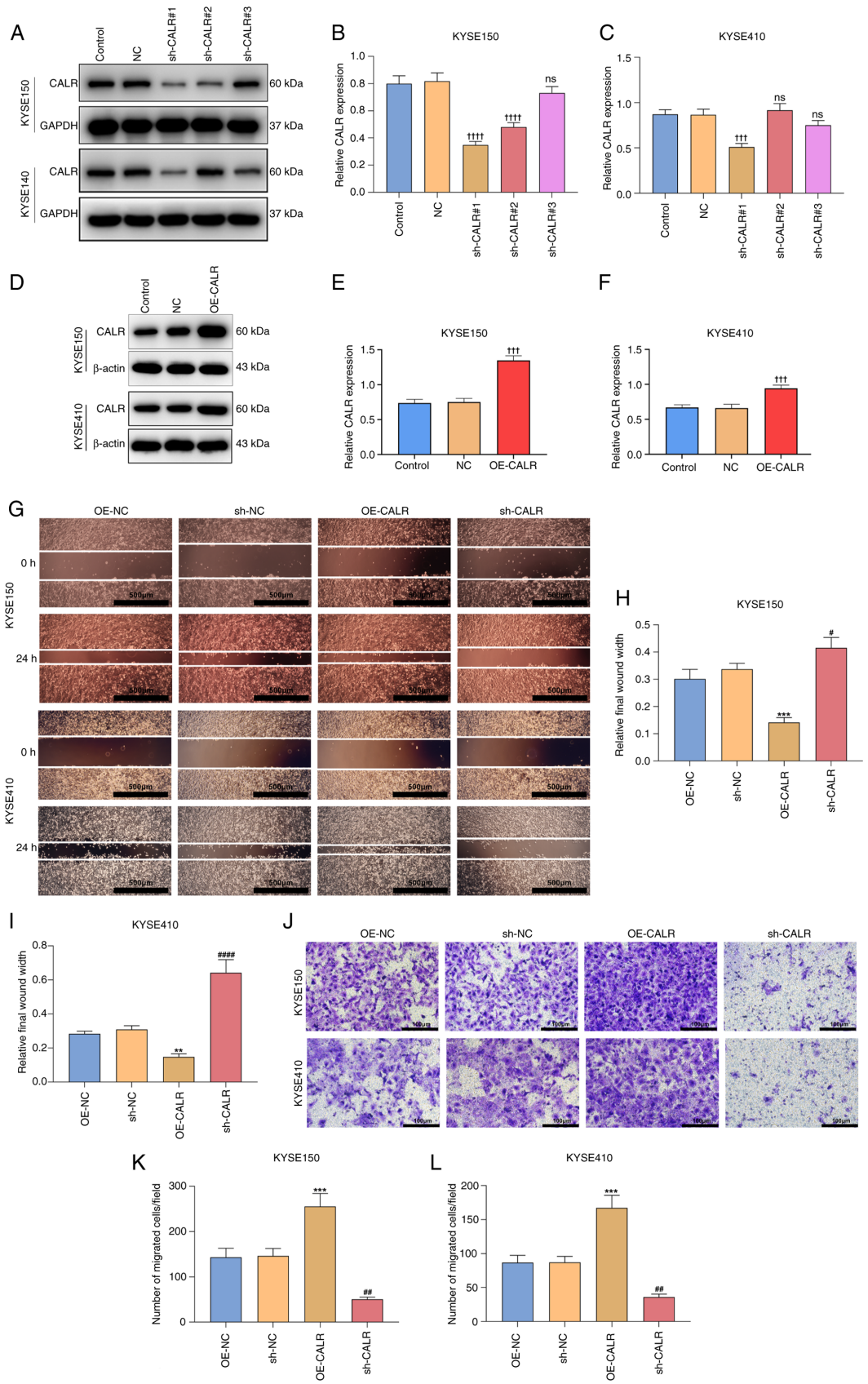

Figure 2. CALR is responsible for esophageal squamous cell carcinoma migration. (A) Western blots of CALR expression in KYSE150 or KYSE410 cells with sh-CALR transfection. (B) Quantification of proteins in KYSE150 cell in each group. (C) Quantification of proteins in KYSE410 cells. (D) Transfection efficiency of CALR overexpression plasmid was verified by western blotting. (E) Quantification of transfection efficiency of KYSE150 cell. (F) Quantification of transfection efficiency of KYSE410 cell. (G) Wound distance at 0 and 24 h for KYSE150 or KYSE410 cells with OE-CALR or sh-CALR transfection. (H) Quantification of relative final wound width in KYSE150 cell. (I) Quantification of relative final wound width in KYSE410 cell. Scale bar, 500 μm. (J) Transwell assay of KYSE150 or KYSE410 cells with OE-CALR or sh-CALR transfections. (K) Number of migrated cells/field in KYSE150 cell. (L) Number of migrated cells/field in KYSE410 cell. Scale bar, 100 μm. ††††P<0.0001, †††P<0.001 vs. NC, **P<0.01, ***P<0.001 vs. OE-NC, $^{\#}$P<0.05, $^{\#\#}$P<0.01, $^{\#\#\#\#}$P<0.0001 vs. sh-NC. CALR, Calreticulin; sh, short hairpin; OE, overexpression; NC, negative control; ns, not significant.

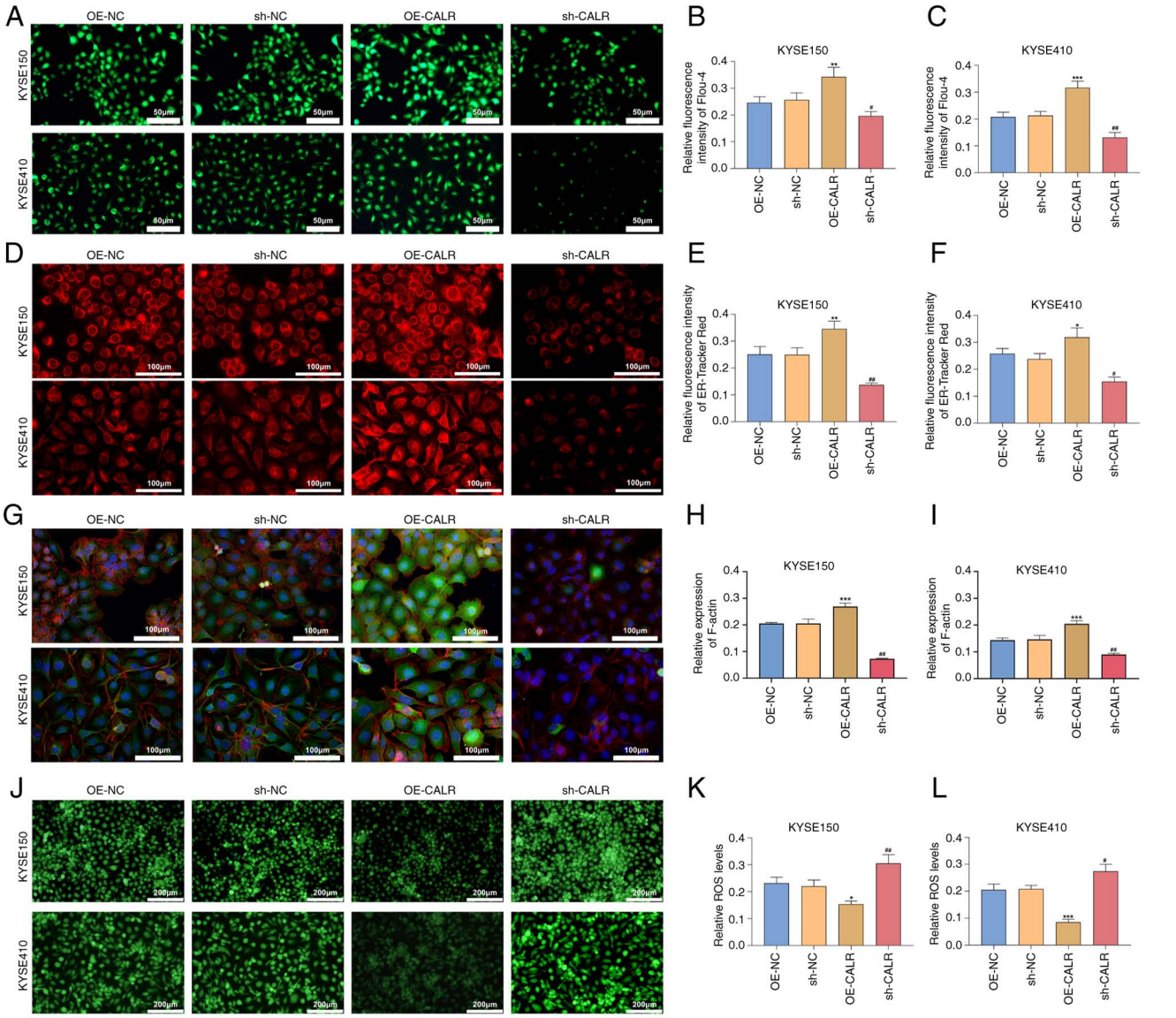

Figure 3. CALR effect on intracellular Ca^{2+} concentration, endoplasmic reticulum stress, cytoskeletal remodeling and ROS accumulation of esophageal squamous cell carcinoma cells. (A) Flou-4 AM fluorescent staining for intracellular Ca^{2+} concentration of KYSE150 or KYSE410 cells with OE-CALR or sh-CALR transfections. Scale bar, 50 μm. (B) Quantification of relative fluorescence intensity of flou-4 in (C) KYSE150. (C) Quantification of relative fluorescence intensity of flou-4 in KYSE410. (D) ER-Tracker Red staining of KYSE150 or KYSE410 cell line with OE-CALR or sh-CALR transfection. Scale bar, 100 μm. (E) Quantification of relative fluorescence intensity of ER-Tracker Red in KYSE150. (F) Quantification of relative fluorescence intensity of ER-Tracker Red in KYSE410. (G) Cytoskeletal microfilament structure staining, Scale bar, 100 μm. (H) Quantification of relative expression of F-actin in KYSE150. (I) Quantification of relative expression of F-actin in KYSE410. (J) DCFH-DA fluorescent staining for intracellular ROS levels in KYSE150 or KYSE410 cells with OE-CALR or sh-CALR transfection. Scale bar, 200 μm. (K) Relative ROS levels in KYSE150. (L) Relative ROS level in KYSE410. *P<0.05, **P<0.01, ***P<0.001 vs. OE-NC, $^{\#}$P<0.05, $^{\#\#}$P<0.01 vs. sh-NC. CALR, Calreticulin; ROS, reactive oxygen species; OE, overexpression; sh, short hairpin; NC, negative control.

intracellular Ca^{2+} concentration was significantly decreased in KYSE150 or KYSE410 cell lines transfected with sh-CALR. Co-immunoprecipitation showed that CALR overexpression increased the binding between GRP75 and VDAC1, as well as between GRP75 and IP3R1 (Fig. 4M-N). ER fluorescence intensity was enhanced by CALR overexpression and decreased by knockdown (Fig. 3D-F). Moreover, the expression of CALR, CANX and PDIA3 in ESCC cells significantly increased after treatment with ER stress agonist thapsigargin (Fig. 4A-H). GRP78 expression was increased in KYSE150 or KYSE410 cells with OE-CALR transfection compared with controls (Fig. 4I-L). These indicated that CALR induced ER stress of ESCC cells.

CALR enhances remodeling of the cellular cytoskeleton. Following transfection with OE-CALR, the fluorescence intensity of KYSE150 and KYSE410 cells stained with ActinRed was enhanced; the fluorescence intensity decreased after CALR was knocked down (Fig. 3G-I). This suggests that CALR enhanced remodeling of the cellular cytoskeleton.

CALR reduces intracellular ROS accumulation in ESCC cells. Levels of intracellular ROS accumulation were measured using DCFH-DA fluorescent probe. In comparison with controls, OE-CALR transfection decreased intracellular ROS accumulation in KYSE150 or KYSE410 cells (Fig. 3J-L). Moreover, intracellular ROS levels were increased in KYSE150 or

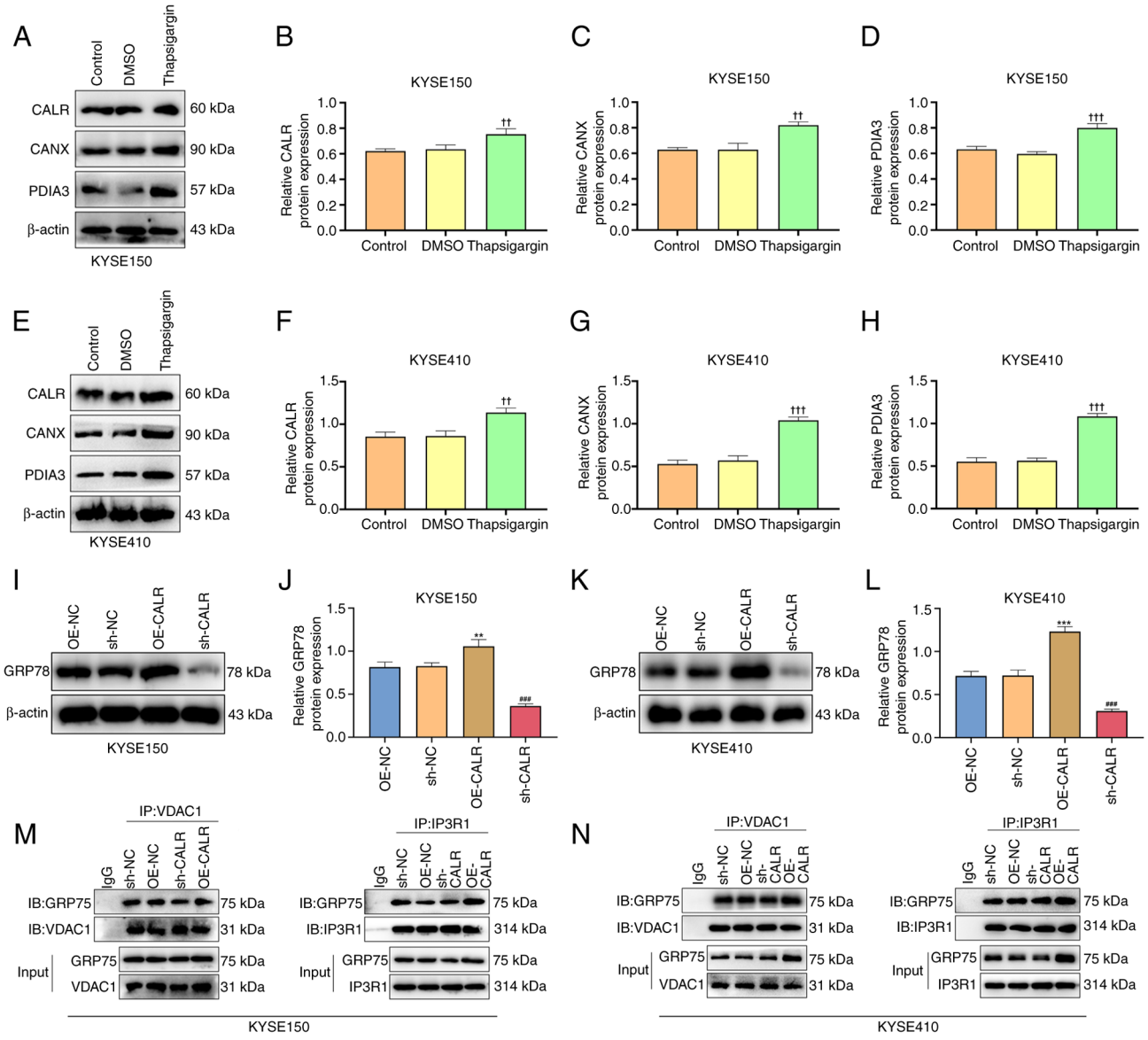

Figure 4. CALR regulates IP3R calcium ion release channels and ER stress. (A) Protein expression of (B) CALR, (C) CANX and (D) PDIA3 in KYSE150 after treatment with ER stress agonist thapsigargin. (E) Protein expression of (F) CALR, (G) CANX and (H) PDIA3 in KYSE410 cells following treatment with ER stress agonist thapsigargin. (I) In intracellular GRP78 expression after overexpression or knockdown of CALR in KYSE150. (J) Protein expression of GRP78 in KYSE150. (K) In intracellular GRP78 expression after overexpression or knockdown of CALR in KYSE410. (L) Protein expression of GRP78 in KYSE410. (M) Co-IP revealed the interaction of GRP75 and VDAC1 and IP3R1 in KYSE150. (N) Co-IP revealed the interaction of GRP75 and VDAC1 and IP3R1 in KYSE410. ††P<0.01, †††P<0.001 vs. DMSO, **P<0.01, ***P<0.001 vs. OE-NC, $^{###}$P<0.001 vs. sh-NC. CALR, Calreticulin; IP3R, inositol 1,4,5-Trisphosphate Receptor; ER, endoplasmic reticulum; CANX, calnexin; PDIA3, protein disulfide isomerase A3; ESCC, esophageal squamous cell carcinoma; GRP, glucose regulatory protein; VDAC, voltage-dependent anion channel; IB, immunoblotting; IP, immunoprecipitation; OE, overexpression; NC, negative control; sh, short hairpin.

KYSE410 cells with sh-CALR transfections. Hence, CALR decreased intracellular ROS accumulation in ESCC cells.

CALR increases CANX and PDIA3 expression in ESCC cells. In comparison with controls, OE-CALR-treated KYSE150 or KYSE410 cells exhibited increased expression of CALR, CANX and PDIA3 both in immunohistochemical and immunofluorescent staining (Fig. 5A-N), whereas expression levels were decreased in KYSE150 or KYSE410 cells with sh-CALR transfection. Western blots demonstrated the enhanced expression of CALR, CANX and PDIA3 in OE-CALR-treated KYSE150 or KYSE410 cells but expression levels were decreased when CALR was knocked out (Fig. 6A-K). Altogether, CALR modulated CANX and PDIA3 expression in ESCC cells.

CALR induces epithelial-mesenchymal transition (EMT) of ESCC cells. Mesenchymal markers vimentin, and N-cadherin were examined through western blots. In comparison with controls, vimentin and N-cadherin expression levels were enhanced in KYSE150 or KYSE410 cells with OE-CALR transfection (Fig. 6A-K).

CALR promotes mitochondrial function of ESCC cells. Mitochondrial membrane potential (indicated by JC-1 staining; Fig. 7A-C) and ratio of NAD^+/NADH content of KYSE150

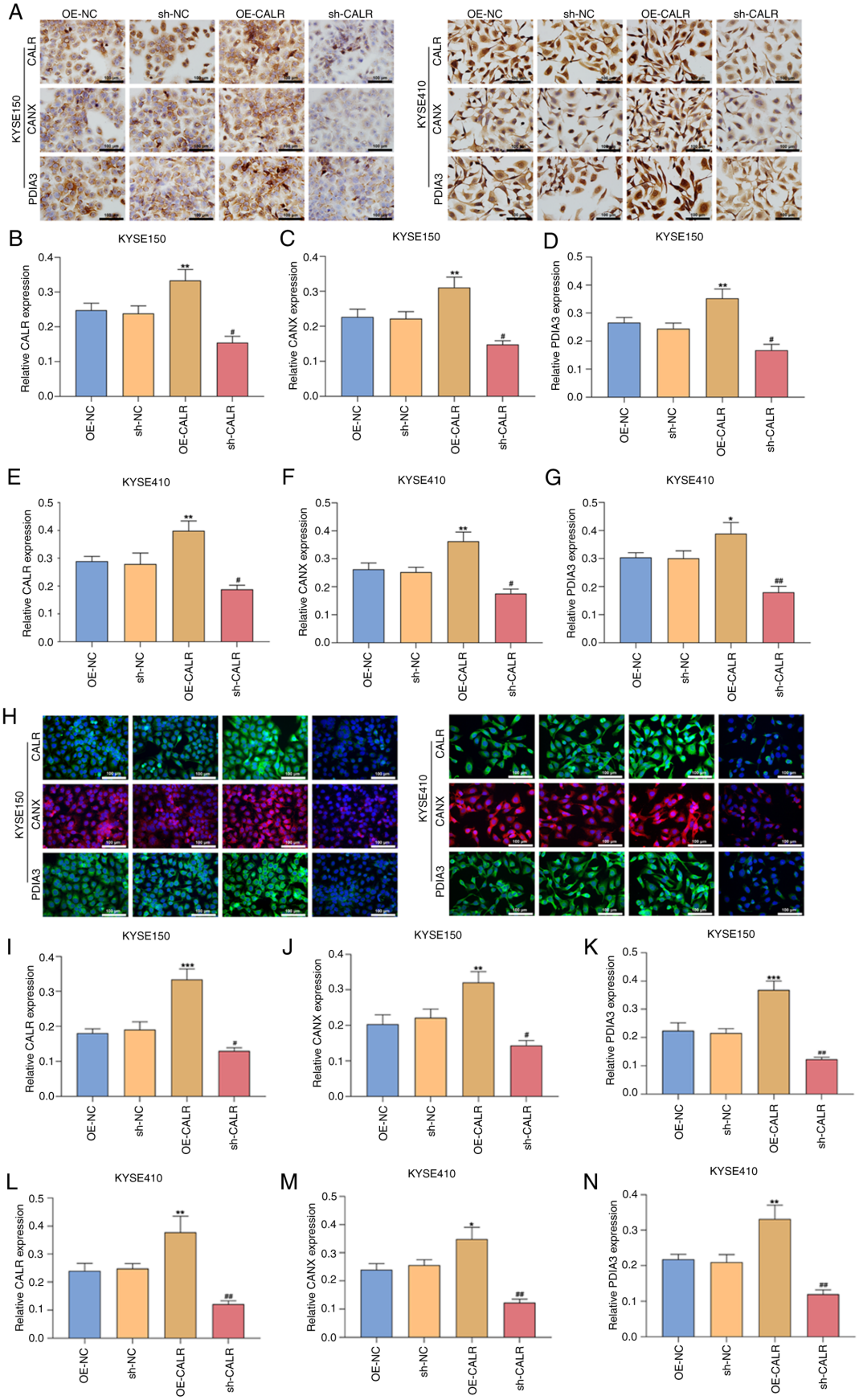

Figure 5. CALR increases CANX and PDIA3 expression in esophageal squamous cell carcinoma cells. (A) Representative immunohistochemical staining. Relative expression of (B) CALR, (C) CANX and (D) PDIA3 in KYSE150, relative expression of (E) CALR, (F) CANX and (G) PDIA3 in KYSE410 following OE-CALR or sh-CALR transfection. (H) Representative immunofluorescent staining. Scale bar, 100 μm. Relative expression of (I) CALR, (J) CANX and (K) PDIA3 in KYSE150, relative expression of (L) CALR, (M) CANX and (N) PDIA3 in KYSE410 with OE-CALR or sh-CALR transfection. *P<0.05, **P<0.01, ***P<0.001 vs. OE-NC, $^{\#}$P<0.05, $^{\#\#}$P<0.01 vs. sh-NC. CALR, calreticulin; CANX, calnexin; PDIA3, protein disulfide isomerase A3; OE, overexpression; sh, short hairpin; NC, negative control.

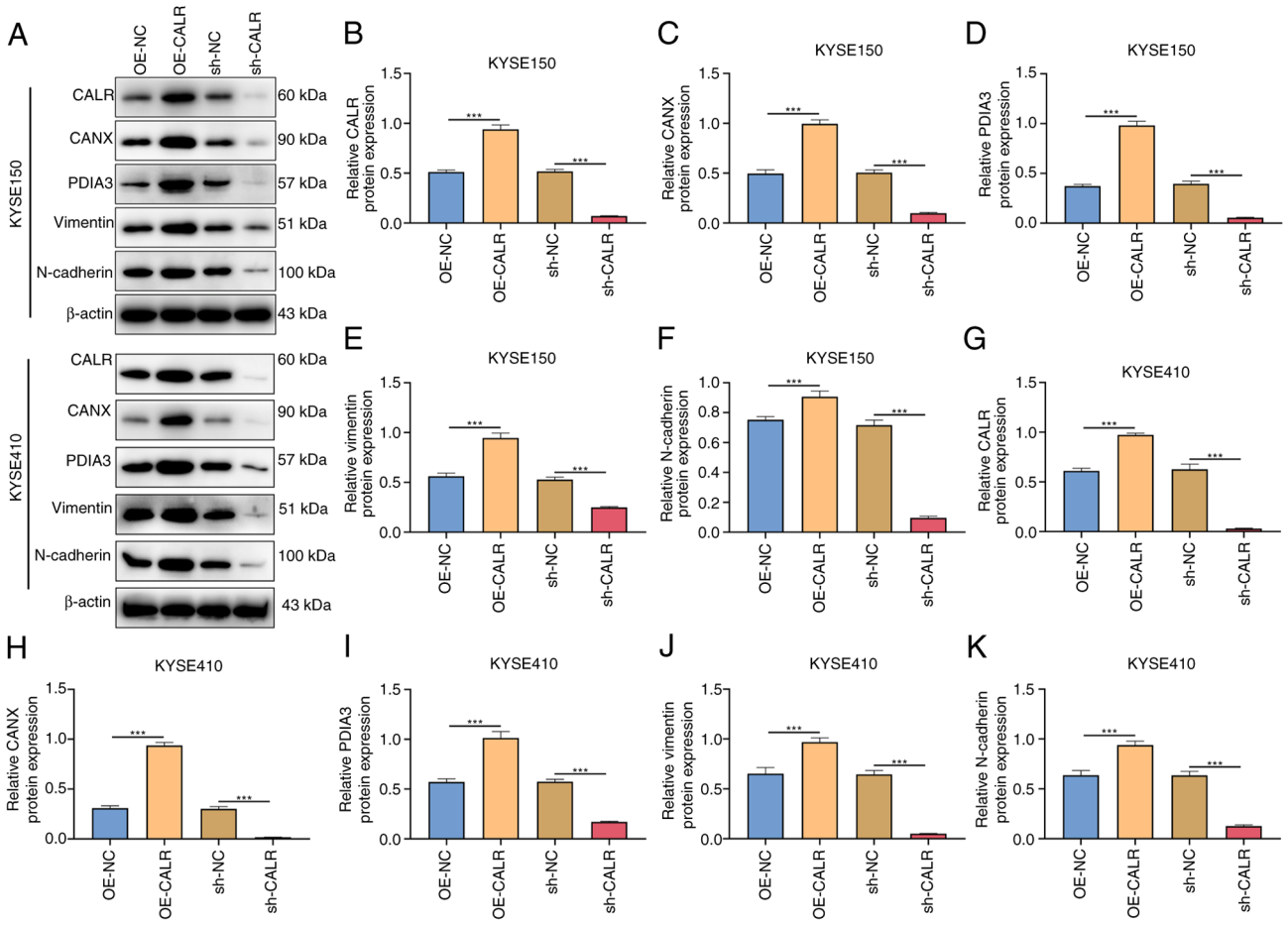

Figure 6. CALR induces epithelial-mesenchymal transition of esophageal squamous cell carcinoma cells. (A) Representative western blots. Relative protein expression of (B) CALR, (C) CANX, (D) PDIA3, (E) vimentin and (F) N-cadherin in KYSE150 with OE-CALR or sh-CALR transfection. Relative protein expression of (G) CALR, (H) CANX, (I) PDIA3, (J) vimentin and (K) N-cadherin in KYSE410 with OE-CALR or sh-CALR transfection. ***P<0.001. CALR, Calreticulin; CANX, calnexin; PDIA3, protein disulfide isomerase A3; OE, overexpression; sh, short hairpin; NC, negative control.

and KYSE410 cells overexpressing CALR was significantly increased, while transfection with sh-CALR had the opposite effect (Fig. 7G and H). Compared with controls, OE-CALR transfection resulted in increased mitochondrial perimeter in KYSE150 or KYSE410 cell lines, demonstrating decreased mitochondrial fission (Fig. 7D-F). Additionally, mitochondrial perimeter was decreased in KYSE150 and KYSE410 cells with sh-CALR transfection. Altogether, CALR may maintain mitochondrial function of ESCC cells.

CALR promotes proliferation and inhibits apoptosis of ESCC cells. The number of proliferating KYSE150 and KYSE410 cells overexpressing CALR increased significantly compared with the control group, but decreased following sh-CALR transfection (Fig. 8A-C). Similarly, in CALR-overexpressing KYSE150 and KYSE410 cells, the number of apoptotic cells was decreased, whereas the number of apoptotic cells increased following sh-CALR transfection (Fig. 8D-F). These results indicated that CALR promoted the proliferation and inhibited apoptosis of esophageal carcinoma cells.

Effect of CALR on tumor growth and expression of tumor-associated fibroblast marker protein in mice. The tumor size of mice injected subcutaneously with CALR knockdown ESCC cells was smaller than that of the control group (Fig. 9A and B), indicating that CALR knockdown inhibited tumor growth. The collagen and reticular fibrosis were more obvious in the control group (Fig. 9C-F). Consistent with the results of the cell experiments, the expression levels of CANX and PDIA3 were also decreased following the knockdown of CALR (Fig. 9G-N). Expression of tumor-associated fibroblast activation markers including α-SMA, FAP, FSP1, PDGFR, and TGF-β was also decreased in mice with CALR knockdown (Fig. 9O-T).

Discussion

Limited treatment options and inadequate understanding of the molecular mechanisms of ESCC progression may lead to poorer survival outcomes for patients with esophageal cancer (25-27). ER stress is considered a novel therapeutic target in cancer progression and associated with overall survival of patients (28). Calcium homeostasis signaling is a key factor in ER stress and CALR is responsible for the proper folding of newly generated glycoproteins within the ER (29). However, it is not clear how CALR regulates the biological behavior of esophageal cancer cells through ER stress. The present results demonstrated CALR upregulation

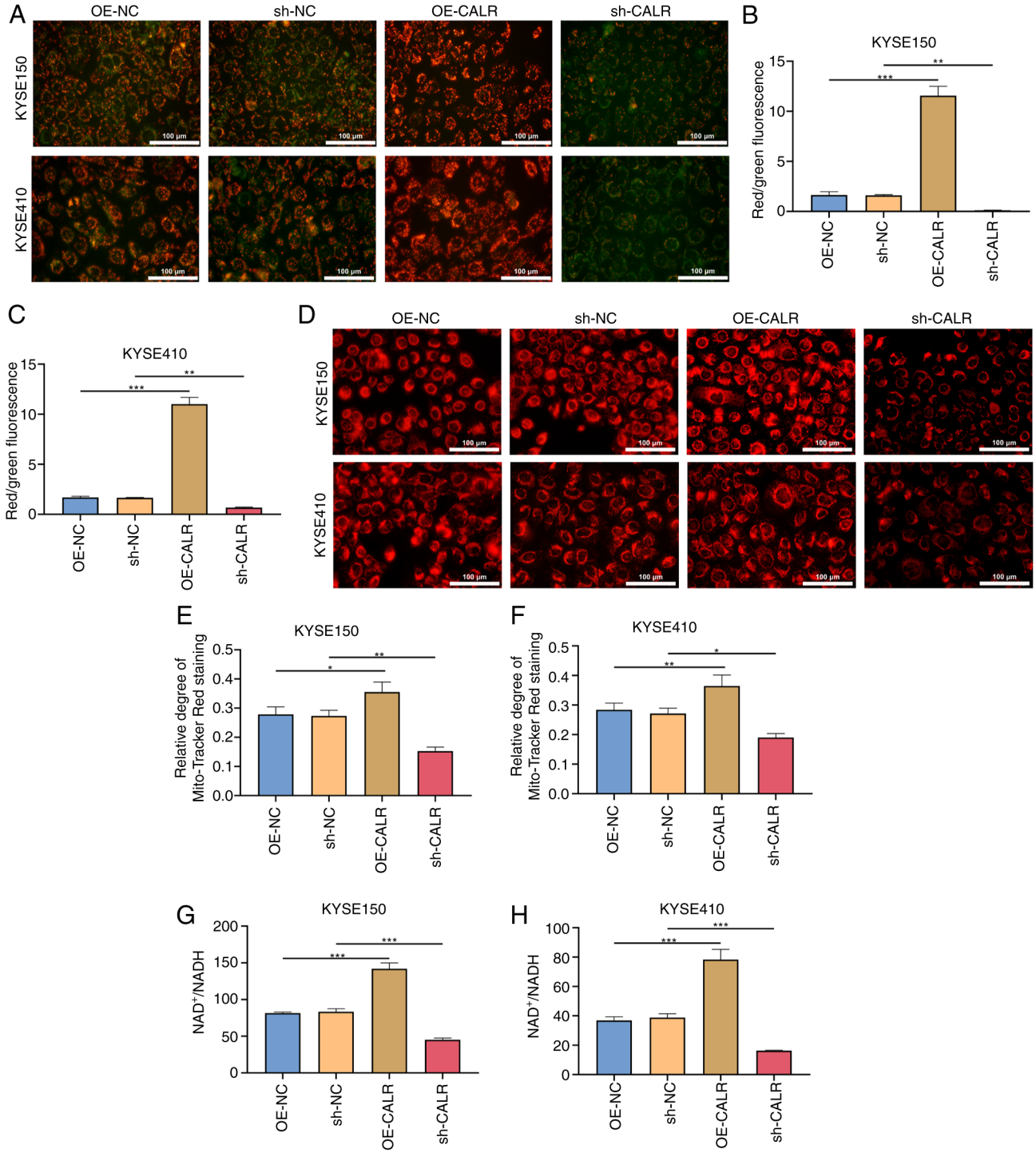

Figure 7. CALR promotes mitochondrial function of ESCC cells. (A) Mitochondrial membrane potential in ESCC cells following transfection with OE-CALR and sh-CALR. Quantification of red (high mitochondrial membrane potential)/green (low mitochondrial membrane potential) fluorescence intensity in (B) KYSE150 and (C) KYSE410. (D) Mito-Tracker Red staining for (E) KYSE150 or (F) KYSE410 cell line with OE-CALR or sh-CALR transfection. Scale bar, 100 μm. Ratio of NAD^+ and NADH content in (G) KYSE150 and (H) KYSE410 cells following transfection with OE-CALR and sh-CALR. *P<0.05, **P<0.01, ***P<0.001. CALR, calreticulin; ESCC, esophageal squamous cell carcinoma; OE, overexpression; sh, short hairpin; NC, negative control.

in clinical ESCC compared with normal esophageal tissues. CALR regulated ESCC cell proliferation and apoptosis, migration capacity, Ca^{2+} accumulation, ER stress, mitochondrial function, and ROS production and cytoskeletal remodeling. CALR knockdown significantly decreased the expression of CANX and PDIA3, inhibited the growth of xenografts and decreased tumor-associated fibroblast levels. In conclusion, the present results suggest that targeting CALR can reduce calcium ion levels and energy metabolism in esophageal cancer cells to induce apoptosis and inhibit ESCC progression.

CALR is involved in cellular processes, including supporting Ca^{2+}-dependent processes to maintain ER function; activating CALR can initiate anti-tumor immunity (30). Increased expression of CALR indicates poor prognosis of nasopharyngeal carcinoma and accelerates cell

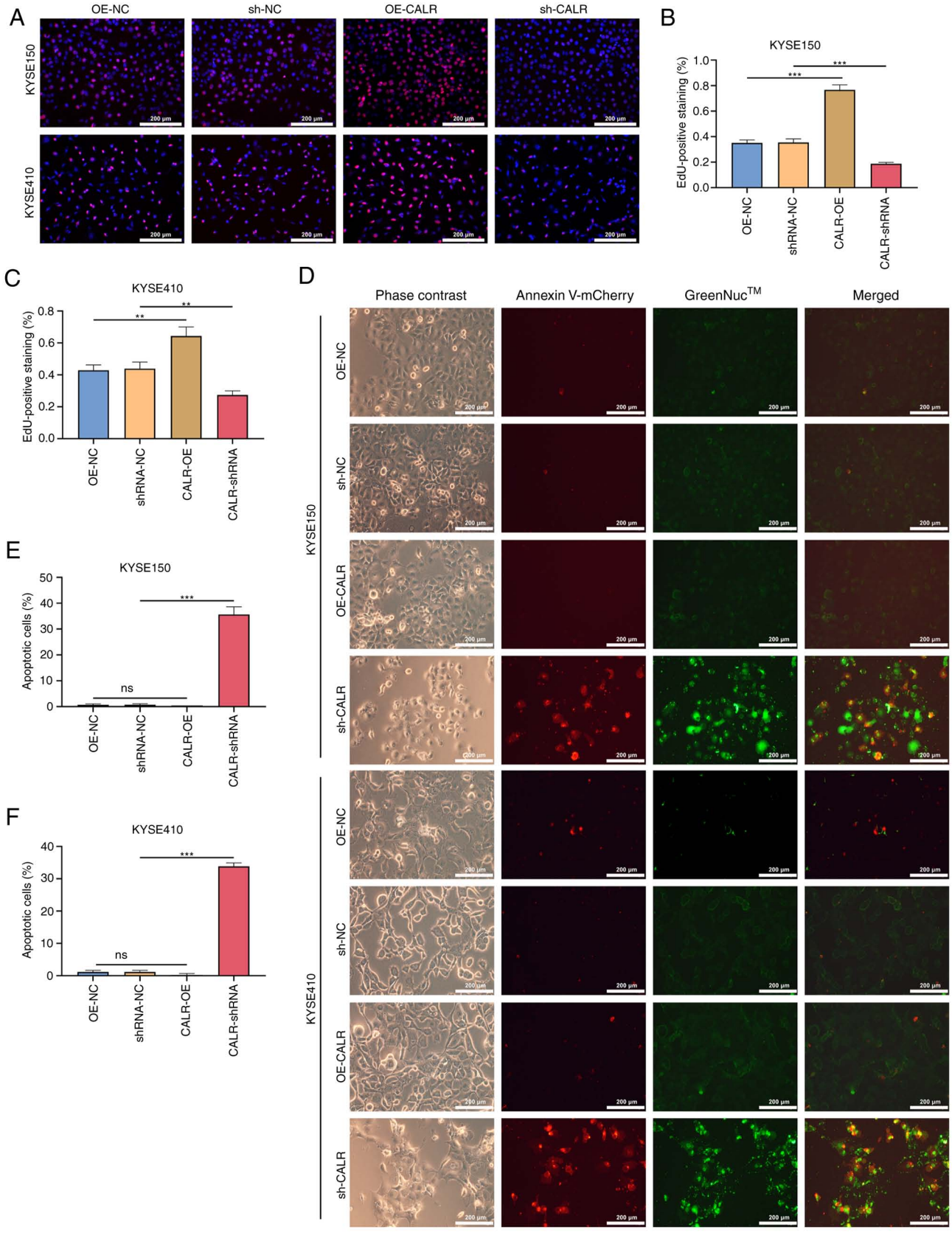

Figure 8. CALR promotes proliferation and inhibits apoptosis of esophageal squamous cell carcinoma cells. (A) EdU staining of proliferated cells. Proportion of proliferated (B) KYSE150 and (C) KYSE410. (D) Staining of apoptotic cells. Scale bar, 200 μm. Proportion of apoptotic cells to total cell number in (E) KYSE150 and (F) KYSE410. **P<0.01, ***P<0.001. CALR, calreticulin; sh, short hairpin; OE, overexpression; NC, negative control; ns, not significant.

migration and invasion via activation of STAT3 (31). CALR regulates intracellular free calcium-dependent chronic ER stress and induces metastasis of pancreatic cancer cells; knockdown CALR reduces subcutaneous tumor size and

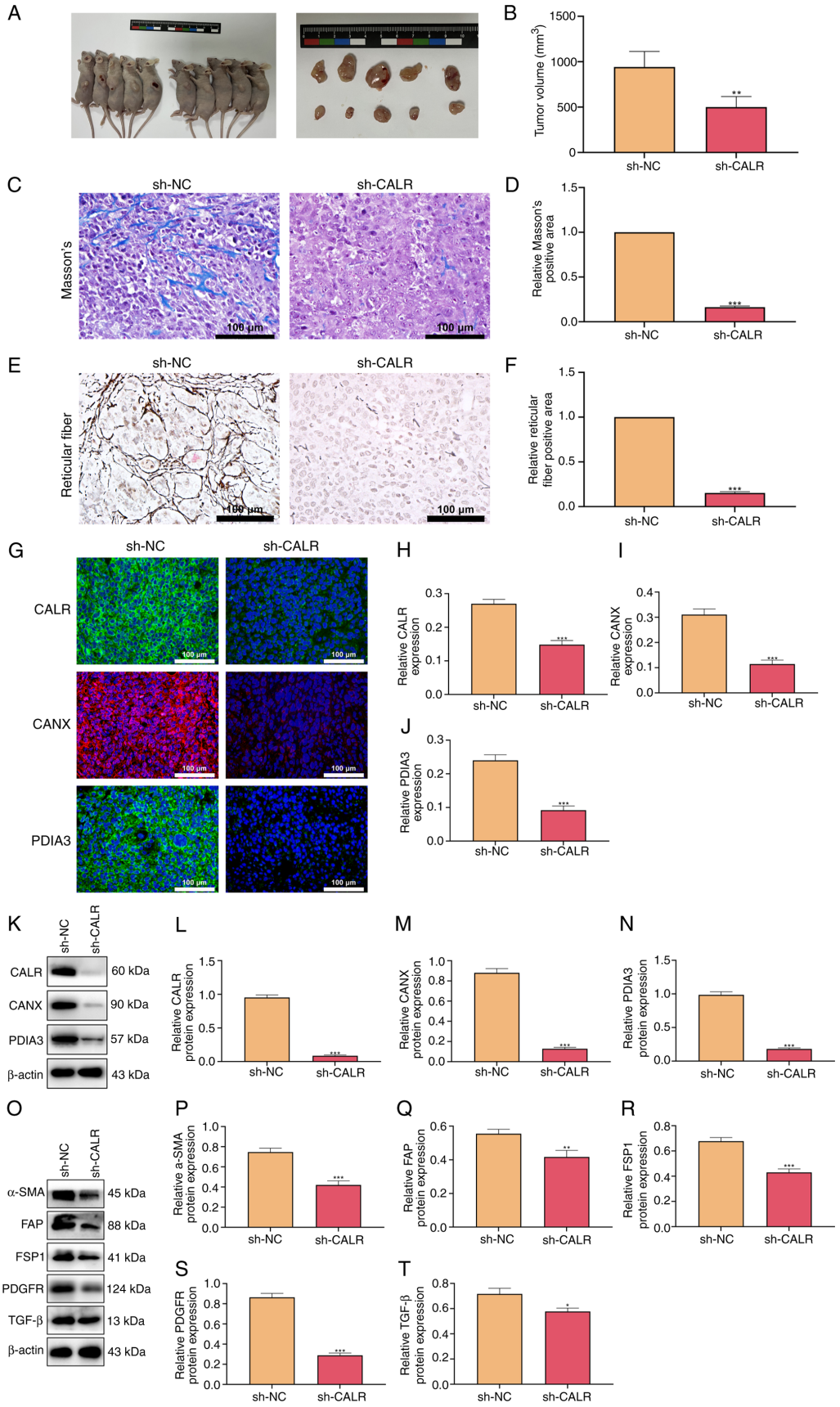

Figure 9. CALR regulates tumor growth and the expression of tumor-associated fibroblast activation marker proteins in mice. (A) Subcutaneous graft. (B) Size of the subcutaneous graft. (C) Staining and (D) quantification of collagen fibers by Masson's staining. (E) Staining and (F) quantification of reticular fibers. (G) Expression of (H) CALR, (I) CANX and (J) PDIA3 detected by immunofluorescent staining. Scale bar, 100 μm. (K) Expression of (L) CALR, (M) CANX and (N) PDIA3 detected by western blotting. (O) Representative western blots. Expression levels of tumor-associated fibroblast activation marker proteins (P) α-SMA, (Q) FAP, (R) FSP1, (S) PDGFR and (T) TGF-β were detected by western blotting. **P<0.01, ***P<0.001. CALR, Calreticulin; CANX, calnexin; PDIA3, protein disulfide isomerase A3; SMA, smooth muscle actin; FAP, fibroblast Activation Protein; FSP1, fibroblast specific protein 1; PDGFR, platelet derived growth factor receptors; sh, short hairpin; NC, negative control.

distant liver metastasis (32). Cell migration is the result of induction of EMT (33). In the present study, EMT markers in esophageal cancer cells were also regulated by CALR and overexpression of CALR upregulated the expression of vimentin and N-cadherin. CALR was found to regulate the proliferation and apoptosis of esophageal cancer cells and decrease the size of subcutaneous implant tumors, indicating the role of CALR in division and proliferation of esophageal cancer cells. Additionally, CALR heightens breast carcinogenesis as well as progression via Wnt/β-catenin signaling activation (34). CALR, a reticular protein, participates in a quality control system for newly synthesized proteins and glycoproteins that relies on other chaperone proteins, including CANX and PDIA3 (11,12). The present study demonstrated that CALR can regulate the expression of CANX and PDIA3, which may associated with Ca^{2+}-dependent processes and ER stress, thus promoting cancer. The CALR/CANX cycle prevents proteins from misfolding (35). In bone marrow-derived dendritic cells, Wntless deficiency leads to ER stress response, increased macroautophagy/autophagy, reduced calcium outflow from ER and disruption of the CALR/CANX cycle, resulting in protein hypoglycation (12). The present study showed that CALR knockdown could reduce CANX expression, hinder CALR/CANX cycling and disrupt ER calcium homeostasis and mitochondrial function.

Intracellular Ca^{2+} serves a key role in ER and mitochondrial homeostasis (36). Ca^{2+} homeostasis is a key factor in tumorigenesis, development and metastasis. Ca^{2+}-dependent proteins of the ER can affect mitochondrial function and ATP production, which is associated with cell apoptosis (37). Targeting abnormal Ca^{2+} signaling in ESCC cells represents a developing therapeutic approach (38). In myeloproliferative tumors, CALR mutation serves as an important marker for molecular pathological diagnosis (39). CALR in mouse and human acute myeloid leukemia cells is induced by activation of AMPK when exposed to the cell surface and acts as a damage-associated molecular pattern to stimulate an immune response (40). In breast cancer, CALR exposure and ATP release are involved in anti-tumor response (41). The present study did not assess tumor immune response but investigated the regulatory role of CALR in esophageal cancer because CALR can affect ATP production by regulating the levels of Ca^{2+} and mitochondrial membrane potential in esophageal cancer cells, which is similar to the aforementioned results, revealing that CALR can regulate mitochondrial ATP production. ROS levels increased after CALR knockdown, promoting apoptosis of esophageal cancer cells and inducing cytoskeletal remodeling. These results highlighted the regulatory role of CALR in ER and mitochondria. It was hypothesized that CALR plays a bridging role between the ER and mitochondria, which is not solely Ca^{2+}-dependent. PDIA3 is a dynamic feature of malignant progression in anaplastic thyroid carcinoma (ATC); CALR exposure and ATP release are the key factors driving malignant progression of ATC (42). Therefore, the role of CALR in regulating mitochondria may be associated with regulation of PDIA3 expression. In future, studies should use cryo-electron microscopy to determine the role of CALR in the connective structure of ER and mitochondria.

Disrupting mitochondrial homeostasis is an anti-neoplastic target in ESCC (43). For example, isocitrate dehydrogenase 2 results in radio-therapeutic resistance in ESCC through heightening mitochondrial function (44). Deferoxamine alleviates ESCC growth through ERK1/2-dependent mitochondrial dysfunction (45). CALR downregulations lead to mitochondrial Ca^{2+} overload and permeability transition pore-mediated cell death in tumor cells (46). Compared with studies of non-small cell lung cancer (NSCLC), the present results are different (19,47-48): In this study, CALR was overexpressed in esophageal cancer cells and promoted the invasion of tumor-associated fibroblasts. However, the level of CALR expression is low in some NSCLCS. Chen *et al* (19) showed that CALR inhibited non-small cell lung cancer progression by facilitating dendritic cell infiltration in NSCLC tissues, Stoll *et al* (47) has detected in a small subset of NSCLC that the loss of CALR expression, those may be due to different tumor tissue sources. Studies have shown that the impact of total or membrane exposure CALR levels on prognosis vary depending on the type of cancer (10,48). As one of the immunogenic cell death hallmarks, previous findings also have shown a significant association between CALR and immune cell infiltration in esophageal cancer: Patients with esophageal cancer with high expression of CALR exhibit longer disease-free survival (49). Transportation of CALR to the plasma membrane surface induces immunogenic cell death. However, the present study only focused on the regulation induced by knocking down the expression of total CALR in cells, which demonstrates that different CALR expression have different effects on cancer cells in different types of tissues and cell, especially in the mechanism of the immune system against cancer. In addition to downregulating the expression of CANX and PDIA3, CALR knockdown also decreased tumor-associated fibroblast levels in mice, accompanied by a decrease expression in fibroblast markers. Cell and mouse experiments showed that CALR mediated cell proliferation and apoptosis and inhibited tumor-related fibroblast infiltration.

In summary, the present study revealed the carcinogenic role of CALR in ESCC. CALR promoted the progression of ESCC by regulating ER stress and mitochondrial function, mediating ATP production, cytoskeletal remodeling, cell proliferation and apoptosis through CANX and PDIA3. Knockdown CALR significantly inhibited tumor-associated fibroblast infiltration and is a potential drug target for ESCC.

Acknowledgements

Not applicable.

Funding

The present study was supported by Natural Science Foundation of Ningxia (grant nos. 2023AAC03529 and 2024AAC03702) and Ningxia Hui Autonomous Region Key Research and Development Project (grant no. 2020BEG03001).

Availability of data and materials

The data generated in the present study may be requested from the corresponding author.

Authors' contributions

YM and WL designed the experiments. XW, YH, LZ, FZ and SY performed experiments. YL, YW and XM wrote and revised the manuscript and analyzed the data. HY, HL and FH analyzed the data. YM and SY confirm the authenticity of all the raw data. All authors have read and approved the final manuscript.

Ethics approval and consent to participate

The present study was performed in accordance with the World Medical Association Declaration of Helsinki and Guidelines for the Care and Use of Laboratory Animals. Approval of the experiments involving patient samples and animals was granted by the Ethics Committee of the General Hospital of Ningxia Medical University (approval no. 2020-880).

Patient consent for publication

Not applicable.

Competing interests

The authors declare that they have no competing interests.

References

1. Bray F, Laversanne M, Sung H, Ferlay J, Siegel RL, Soerjomataram I and Jemal A: Global cancer statistics 2022: GLOBOCAN estimates of incidence and mortality worldwide for 36 cancers in 185 countries. CA Cancer J Clin 74: 229-263, 2024.
2. Liu Z, Gu S, Lu T, Wu K, Li L, Dong C and Zhou Y: IFI6 depletion inhibits esophageal squamous cell carcinoma progression through reactive oxygen species accumulation via mitochondrial dysfunction and endoplasmic reticulum stress. J Exp Clin Cancer Res 39: 144, 2020.
3. Huang J, Xu J, Chen Y, Zhuang W, Zhang Y, Chen Z, Chen J, Zhang H, Niu Z, Fan Q, *et al*: Camrelizumab versus investigator's choice of chemotherapy as second-line therapy for advanced or metastatic oesophageal squamous cell carcinoma (ESCORT): A multicentre, randomised, open-label, phase 3 study. Lancet Oncol 21: 832-842, 2020.
4. Wang H, Tang H, Fang Y, Tan L, Yin J, Shen Y, Zeng Z, Zhu J, Hou Y, Du M, *et al*: Morbidity and mortality of patients who underwent minimally invasive esophagectomy after neoadjuvant chemoradiotherapy vs. neoadjuvant chemotherapy for locally advanced esophageal squamous cell carcinoma: A randomized clinical trial. JAMA Surg 156: 444-451, 2021.
5. Doki Y, Ajani JA, Kato K, Xu J, Wyrwicz L, Motoyama S, Ogata T, Kawakami H, Hsu CH, Adenis A, *et al*: Nivolumab combination therapy in advanced esophageal squamous-cell carcinoma. N Engl J Med 386: 449-462, 2022.
6. Wang ZX, Cui C, Yao J, Zhang Y, Li M, Feng J, Yang S, Fan Y, Shi J, Zhang X, *et al*: Toripalimab plus chemotherapy in treatment-naïve, advanced esophageal squamous cell carcinoma (JUPITER-06): A multi-center phase 3 trial. Cancer Cell 40: 277-288.e3, 2022.
7. Yamamoto S and Kato K: JUPITER-06 establishes immune checkpoint inhibitors as essential first-line drugs for the treatment of advanced esophageal squamous cell carcinoma. Cancer Cell 40: 238-240, 2022.
8. Ma F, Li Y, Xiang C, Wang B, Lv J, Wei J, Qin Z, Pu Y, Li K, Teng H, *et al*: Proteomic characterization of esophageal squamous cell carcinoma response to immunotherapy reveals potential therapeutic strategy and predictive biomarkers. J Hematol Oncol 17: 11, 2024.
9. Miao Z, Li J, Zeng S, Lv Y, Jia S, Ding D, Li W and Liu Q: Endoplasmic reticulum-targeting AIE photosensitizers to boost immunogenic cell death for immunotherapy of bladder carcinoma. ACS Appl Mater Interfaces 16: 245-260, 2024.
10. Fucikova J, Spisek R, Kroemer G and Galluzzi L: Calreticulin and cancer. Cell Res 31: 5-16, 2021.
11. Fabarius A, Samra V, Drews O, Mörz H, Bierbaum M, Darwich A, Weiss C, Brendel S, Kleiner H, Seifarth W, *et al*: Evidence for recombinant GRP78, CALR, PDIA3 and GPI as mediators of genetic instability in human CD34+ cells. Cancers (Basel) 14: 2883, 2022.
12. Wang LT, Lin MH, Liu KY, Chiou SS, Wang SN, Chai CY, Tseng LW, Chiou HC, Wang HC, Yokoyama KK, *et al*: WLS/wntless is essential in controlling dendritic cell homeostasis via a WNT signaling-independent mechanism. Autophagy 17: 4202-4217, 2021.
13. da Silva DC, Valentão P, Andrade PB and Pereira DM: Endoplasmic reticulum stress signaling in cancer and neurodegenerative disorders: Tools and strategies to understand its complexity. Pharmacol Res 155: 104702, 2020.
14. Antoniotti V, Bellone S, Correia FP, Peri C, Tini S, Ricotti R, Mancioppi V, Gagliardi M, Spadaccini D, Caputo M, *et al*: Calreticulin and PDIA3, two markers of endoplasmic reticulum stress, are associated with metabolic alterations and insulin resistance in pediatric obesity: A pilot study. Front Endocrinol (Lausanne) 13: 1003919, 2022.
15. Khan AA, Allemailem KS, Almatroudi A, Almatroodi SA, Mahzari A, Alsahli MA and Rahmani AH: Endoplasmic reticulum stress provocation by different nanoparticles: An innovative approach to manage the cancer and other common diseases. Molecules 25: 5336, 2020.
16. Li J, Qi F, Su H, Zhang C, Zhang Q, Chen Y, Chen P, Su L, Chen Y, Yang Y, *et al*: GRP75-faciliated mitochondria-associated ER membrane (MAM) integrity controls cisplatin-resistance in ovarian cancer patients. Int J Biol Sci 18: 2914-2931, 2022.
17. Li X, Zhao X, Qin Z, Li J, Sun B and Liu L: Regulation of calcium homeostasis in endoplasmic reticulum-mitochondria crosstalk: Implications for skeletal muscle atrophy. Cell Commun Signal 23: 17, 2025.
18. Lee SY, Oh JY, Kang TH, Shin HS, Cheng MA, Farmer E, Wu TC and Hung CF: Endoplasmic reticulum stress enhances the antigen-specific T cell immune responses and therapeutic antitumor effects generated by therapeutic HPV vaccines. J Biomed Sci 26: 41, 2019.
19. Chen R, Huang M, Yang X, Chen XH, Shi MY, Li ZF, Chen ZN and Wang K: CALR-TLR4 complex inhibits non-small cell lung cancer progression by regulating the migration and maturation of dendritic cells. Front Oncol 11: 743050, 2021.
20. Fucikova J, Kepp O, Kasikova L, Petroni G, Yamazaki T, Liu P, Zhao L, Spisek R, Kroemer G and Galluzzi L: Detection of immunogenic cell death and its relevance for cancer therapy. Cell Death Dis 11: 1013, 2020.
21. Niu X, Chen L, Li Y, Hu Z and He F: Ferroptosis, necroptosis, and pyroptosis in the tumor microenvironment: Perspectives for immunotherapy of SCLC. Semin Cancer Biol 86: 273-285, 2022.
22. Liu X, Song N, Liu Y, Liu Y, Li J, Ding J and Tong Z: Efficient induction of anti-tumor immune response in esophageal squamous cell carcinoma via dendritic cells expressing MAGE-A3 and CALR antigens. Cell Immunol 295: 77-82, 2015.
23. Wang X, Song X, Cheng G, Zhang J, Dong L, Bai J, Luo D, Xiong Y, Li S, Liu F, *et al*: The regulatory mechanism and biological significance of mitochondrial calcium uniporter in the migration, invasion, angiogenesis and growth of gastric cancer. Onco Targets Ther 13: 11781-11794, 2020.
24. Tang Z, Kang B, Li C, Chen T and Zhang Z: GEPIA2: An enhanced web server for large-scale expression profiling and interactive analysis. Nucleic Acids Res 47: W556-W560, 2019.
25. Pelosof L, Saung MT, Donoghue M, Casak S, Mushti S, Cheng J, Jiang X, Liu J, Zhao H, Khazraee M, *et al*: Benefit-Risk summary of nivolumab for the treatment of patients with unresectable advanced, recurrent, or metastatic esophageal squamous cell carcinoma after prior fluoropyrimidine- and platinum-based chemotherapy. Oncologist 26: 318-324, 2021.
26. Sugimura K, Miyata H, Tanaka K, Makino T, Takeno A, Shiraishi O, Motoori M, Yamasaki M, Kimura Y, Hirao M, *et al*: Multicenter randomized phase 2 trial comparing chemoradiotherapy and docetaxel plus 5-fluorouracil and cisplatin chemotherapy as initial induction therapy for subsequent conversion surgery in patients with clinical T4b esophageal cancer: Short-term results. Ann Surg 274: e465-e472, 2021.
27. Yamamoto S, Kawakami H, Kii T, Hara H, Kawabata R, Kawada J, Takeno A, Matsuyama J, Ueda S, Okita Y, *et al*: Randomized phase II study of docetaxel versus paclitaxel in patients with esophageal squamous cell carcinoma refractory to fluoropyrimidine- and platinum-based chemotherapy: OGSG1201. Eur J Cancer 154: 307-315, 2021.

28. Chen H, Xu N, Xu J, Zhang C, Li X, Xu H, Zhu W, Li J, Liang D and Zhou W: A risk signature based on endoplasmic reticulum stress-associated genes predicts prognosis and immunity in pancreatic cancer. Front Mol Biosci 10: 1298077, 2023.
29. Ciftciler R and Balasar O: A rare CALR variant mutation and efficient peginterferon alfa-2a response in a patient with essential thrombocythemia. Cancer Genet 274-275: 51-53, 2023.
30. Ye J, Qi L, Du Z, Yu L, Chen K, Li R, Feng R and Zhai W: Calreticulin: A potential diagnostic and therapeutic biomarker in gallbladder cancer. Aging (Albany NY) 13: 5607-5620, 2021.
31. Han Y, Liao Q, Wang H, Rao S, Yi P, Tang L, Tian Y, Oyang L, Wang H, Shi Y and Zhou Y: High expression of calreticulin indicates poor prognosis and modulates cell migration and invasion via activating Stat3 in nasopharyngeal carcinoma. J Cancer 10: 5460-5468, 2019.
32. Sheng W, Wang G, Tang J, Shi X, Cao R, Sun J, Lin YH, Jia C, Chen C, Zhou J and Dong M: Calreticulin promotes EMT in pancreatic cancer via mediating Ca(2+) dependent acute and chronic endoplasmic reticulum stress. J Exp Clin Cancer Res 39: 209, 2020.
33. Wang L, Chen J, Zuo Q, Wu C, Yu T, Zheng P, Huang H, Deng J, Fang L, Liu H, *et al*: Calreticulin enhances gastric cancer metastasis by dimethylating H3K9 in the E-cadherin promoter region mediating by G9a. Oncogenesis 11: 29, 2022.
34. Liu X, Xie P, Hao N, Zhang M, Liu Y, Liu P, Semenza GL, He J and Zhang H: HIF-1-regulated expression of calreticulin promotes breast tumorigenesis and progression through Wnt/β-catenin pathway activation. Proc Natl Acad Sci USA 118: e2109144118, 2021.
35. Lam STT and Lim CJ: Cancer biology of the endoplasmic reticulum lectin chaperones calreticulin, calnexin and PDIA3/ERp57. Prog Mol Subcell Biol 59: 181-196, 2021.
36. Liu Y, Liu Z and Wang K: The Ca(2+)-activated chloride channel ANO1/TMEM16A: An emerging therapeutic target for epithelium-originated diseases? Acta Pharm Sin B 11: 1412-1433, 2021.
37. Song LL, Qu YQ, Tang YP, Chen X, Lo HH, Qu LQ, Yun YX, Wong VKW, Zhang RL, Wang HM, *et al*: Hyperoside alleviates toxicity of β-amyloid via endoplasmic reticulum-mitochondrial calcium signal transduction cascade in APP/PS1 double transgenic Alzheimer's disease mice. Redox Biol 61: 102637, 2023.
38. Chang Y, Funk M, Roy S, Stephenson E, Choi S, Kojouharov HV, Chen B and Pan Z: Developing a mathematical model of intracellular calcium dynamics for evaluating combined anticancer effects of afatinib and RP4010 in esophageal cancer. Int J Mol Sci 23: 1763, 2022.
39. Andrews C, Conneally E and Langabeer SE: Molecular diagnostic criteria of myeloproliferative neoplasms. Expert Rev Mol Diagn 23: 1077-1090, 2023.
40. Mondesir J, Ghisi M, Poillet L, Bossong RA, Kepp O, Kroemer G, Sarry JE, Tamburini J and Lane AA: AMPK activation induces immunogenic cell death in AML. Blood Adv 7: 7585-7596, 2023.
41. Calvillo-Rodríguez KM, Mendoza-Reveles R, Gómez-Morales L, Uscanga-Palomeque AC, Karoyan P, Martínez-Torres AC and Rodríguez-Padilla C: PKHB1, a thrombospondin-1 peptide mimic, induces anti-tumor effect through immunogenic cell death induction in breast cancer cells. Oncoimmunology 11: 2054305, 2022.
42. Xu T, Zhu C, Song F, Zhang W, Yuan M, Pan Z and Huang P: Immunological characteristics of immunogenic cell death genes and malignant progression driving roles of TLR4 in anaplastic thyroid carcinoma. BMC Cancer 23: 1131, 2023.
43. Yamashita K, Miyata H, Makino T, Masuike Y, Furukawa H, Tanaka K, Miyazaki Y, Takahashi T, Kurokawa Y, Yamasaki M, *et al*: High expression of the mitophagy-related protein pink1 is associated with a poor response to chemotherapy and a poor prognosis for patients treated with neoadjuvant chemotherapy for esophageal squamous cell carcinoma. Ann Surg Oncol 24: 4025-4032, 2017.
44. Chen X, Zhuo S, Xu W, Chen X, Huang D, Sun X and Cheng Y: Isocitrate dehydrogenase 2 contributes to radiation resistance of oesophageal squamous cell carcinoma via regulating mitochondrial function and ROS/pAKT signalling. Br J Cancer 123: 126-136, 2020.
45. Lan L, Wei W, Zheng Y, Niu L, Chen X, Huang D, Gao Y, Mo S, Lu J, Guo M, *et al*: Deferoxamine suppresses esophageal squamous cell carcinoma cell growth via ERK1/2 mediated mitochondrial dysfunction. Cancer Lett 432: 132-143, 2018.
46. Han A, Li C, Zahed T, Wong M, Smith I, Hoedel K, Green D and Boiko AD: Calreticulin is a critical cell survival factor in malignant neoplasms. PLoS Biol 17: e3000402, 2019.
47. Stoll G, Iribarren K, Michels J, Leary A, Zitvogel L, Cremer I and Kroemer G: Calreticulin expression: Interaction with the immune infiltrate and impact on survival in patients with ovarian and non-small cell lung cancer. Oncoimmunology 5: e1177692, 2016.
48. Méndez-Ferrer S, Bonnet D, Steensma DP, Hasserjian RP, Ghobrial IM, Gribben JG, Andreeff M and Krause DS: Bone marrow niches in haematological malignancies. Nat Rev Cancer 20: 285-298, 2020.
49. Luo H, Sun Y, Wang L, Liu H, Zhao R, Song M and Ge H: Targeting endoplasmic reticulum associated degradation pathway combined with radiotherapy enhances the immunogenicity of esophageal cancer cells. Cancer Biol Ther 24: 2166763, 2023.